# Control over the shell thickness of core/shell drops in three-phase glass capillary devices

# Control over the shell thickness of core/shell drops in three-phase glass capillary devices

**Goran T. Vladisavljević[1,2] · Ho Cheung. Shum[3] · David A. Weitz[4]**
[1]Department of Chemical Engineering, Loughborough University, Loughborough, LE11 3TU, UK; [2]Vinča Institute of Nuclear Sciences, PO Box 522, Belgrade, Serbia, [3]Department of Mechanical Engineering, University of Hong Kong, Hong Kong; [4]Department of Physics, Harvard University, MA 02138, USA.

## Abstract

Monodisperse core/shell drops with aqueous core and poly(dimethylsiloxane) (PDMS) shell of controllable thickness have been produced using a glass microcapillary device that combines co-flow and flow-focusing geometries. The throughput of the droplet generation was high, with droplet generation frequency in the range from 1,000 to 10,000 Hz. The size of the droplets can be tuned by changing the flow rate of the continuous phase. The technique enables control over the shell thickness through adjusting the flow rate ratio of the middle to inner phase. As the flow rate of the middle and inner phase increases, the droplet breakup occurs in the dripping-to-jetting transition regime, with each double emulsion droplet containing two monodisperse internal aqueous droplets. The resultant drops can be used subsequently as templates for monodisperse polymer capsules with a single or multiple inner compartments, as well as functional vesicles such as liposomes, polymersomes and colloidosomes.

**Key words** Core/shell drops · polydimethylsiloxane shell · Capillary microfluidics · Functional vesicles · monodisperse particles · Flow focusing

## 1 Introduction

Droplets with a core/shell structure can be used as templates for the production of hollow particles, such as poly(lactic acid) microbubbles [1], hydrogel shells [2] and liquid crystal shells [3], as well as vesicles, such as liposomes [4], polymersomes [5] and colloidosomes [6]. Conventional techniques for vesicle preparation (e.g. rehydration of dried amphiphilic films and electroforming) rely on the self-assembly of amphiphiles under shear and electric field, respectively [7]. However, the resultant vesicles are often non-uniform in size and structure due to the random nature of the self-assembly process. In addition, encapsulation yields of active materials are relatively low [8]. With microfluidic core/shell droplets as templates, vesicles can be prepared via directed assembly of the amphiphiles with higher degree of control over the droplet size and size uniformity as well as improved encapsulation efficiency. Regarding other core/shell

* Corresponding Author: Goran Vladisavljević, e-mail: G.Vladisavljevic@lboro.ac.uk

particles, conventional techniques include internal phase separation [9], complex coacervation [10], layer-by-layer deposition [11] and interfacial polymerization [12]; these typically require multi-stage processing, very specific emulsion formulation, and does not allow close control over the shell thickness. The control over the shell thickness of core/shell particles is highly relevant, because it affects their robustness, mechanical properties and permeability to different species. Poly(dimethylsiloxane) (PDMS) microfluidic devices containing sequential junctions with alternating wettability have been used to generate controllable multiple emulsions [13]. However, PDMS swells in strong organic solvents and has inherently unstable surface properties. In addition, due to its high elasticity, PDMS channels tend to deform with applied pressure. In this work, monodisperse multiple emulsion droplets of different morphology (core/shell or with two inner droplets per each outer drop) have been produced using glass capillary microfluidics [14, 15]. Glass is more chemically robust than PDMS, does not swell, and can easily be functionalized to control surface properties. The aim of the research was to investigate the effect of fluid flow rates on droplet size, morphology, and shell thickness.

**2 Experimental**

Controllable multiple emulsions were produced using microcapillary device shown in Figure 1. The device consists of two round capillaries with a tapered end inserted into a square capillary. First, a round glass capillary (World Precision Instrument, Inc., Sarasota, FL) with an outer diameter of 1 mm and in inner diameter of 0.58 mm was heated and pulled using a Sutter Instrument model P-97 micropipette puller. As a result of the pulling process, the capillary breaks into two parts, each with a tapered end that culminates in a fine orifice. The orifice in both capillaries was then enlarged to the desired diameter by microforging using a Narishige model MF-830 microforge. Capillaries with the desired orifice size were then inserted into a square glass capillary (Vitrocom, Fiber Optic Center, Inc., New Bredford, MA) and glued together on a microscope glass slide. Coaxial alignment of the capillaries was ensured by choosing the capillaries such that the outer diameter of the round capillaries matches the inner dimension of the square capillary. Milli-q water (the inner fluid) was introduced through the injection tube and a solution of 2 % (w/w) Dow Corning 749 Fluid in 10 cP PDMS (the middle fluid) was supplied co-currently through the square capillary. 2 % (w/w) poly(vinyl alcohol) aqueous solution was supplied from the opposite side through the square capillary and all phases were forced into the collection tube. It resulted in the rupture of coaxial jet composed of the inner and middle fluid and formation of droplets, as shown in Figure 1a. In order to prevent wetting of the injection tube with water, the tapered region of the injection tube

was rendered hydrophobic with octadecyltrimethoxysilane. All liquids were delivered to the device from gas tight syringes using separate Harvard Apparatus PHD 22/2000 syringe pumps interfaced to a PC computer. The drop generation process was observed in real time and recorded using a Phantom v7.0 fast speed camera (Vision Research, Inc., USA) attached to a Leica DMIRB inverted microscope.

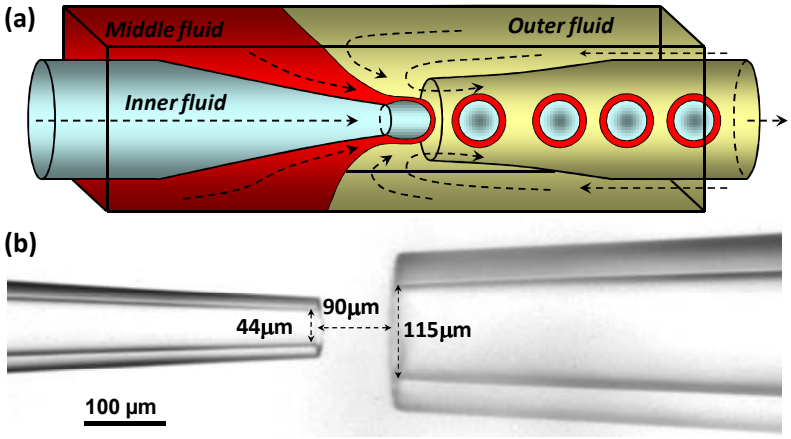


**Figure 1** (a) Schematic of the glass capillary device used in this work; (b) Micrograph of the tapered end of the injection and collection tube. The diameter of the orifice in the injection and collection tube was 44 and 115 µm, respectively and the distance between the ends of the two capillaries was 90 µm.

### 3 Droplet size and generation frequency

In the dripping regime, the interfacial tension between the middle and outer fluid dominates the droplet breakup process [16] and the double emulsions generated had one internal aqueous drop (Figure 2a). As the inertial force of the middle and inner phases becomes comparable to the interfacial tension, the droplet breakup occurs in the dripping-to-jetting transition regime. Each double emulsion droplet formed in this regime had two monodisperse internal aqueous droplets, as shown in Figure 2b. Drops with two inner droplets can be used as templates for fabrication of vesicles with multiple inner compartments, for example multi-compartment colloidosomes [17] or alternatively, dimer particles can be produced, if inner droplets are polymerized.

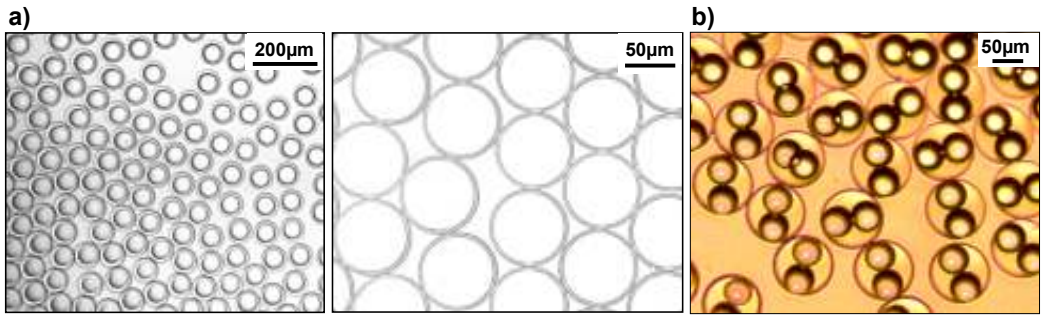


**Figure 2** (a) Micrographs of core/shell droplets with $d_o$ = 78 µm and $\delta$ = 8 µm taken under different magnification; (b) Micrograph of multiple emulsion droplets containing two inner drops.

The diameter, $d_o$ and generation frequency, $\nu$ of the droplets were controlled by changing the flow rate of the continuous phase, $Q_o$ in the range from 10 to 45 ml $h^{-1}$ while keeping the constant flow rate of the middle and inner phase. At $Q_i$ = 4 and $Q_m$ = 1 ml $h^{-1}$, the drop generation frequency was in the range from 1,000 to 10,000 Hz and the droplet diameter varied widely between 60 and 150 μm, as shown in Figure 3. The droplets in this size range can be useful for subcutaneous drug release [18]. As $Q_o$ increases, the viscous drag force between the outer and middle phase increases causing the droplets to detach sooner from the injection tube. As a result, smaller droplets are produced at higher frequencies. The drop generation frequency was nearly 10,000 Hz at $Q_o$ = 45 ml $h^{-1}$. Above that threshold value, the middle fluid forms a long jet, which breaks farther downstream. This regime results in the formation of polydisperse droplets because the point at which a drop separates from the jet can vary. A mass balance for the drop generation process in the dripping regime gives:

$$d_o = [6(Q_m + Q_i)/(\pi \nu)]^{1/3} \quad (1)$$

The drop diameters calculated from Eq. (1) were consistent with the experimental $d_o$ values estimated from microscopic images, as shown in Fig. 3. Eq. (1) shows that $d_o$ is proportional to $\nu^{-1/3}$ at constant $Q_m$ and $Q_i$ values, which is confirmed in Figure 3.

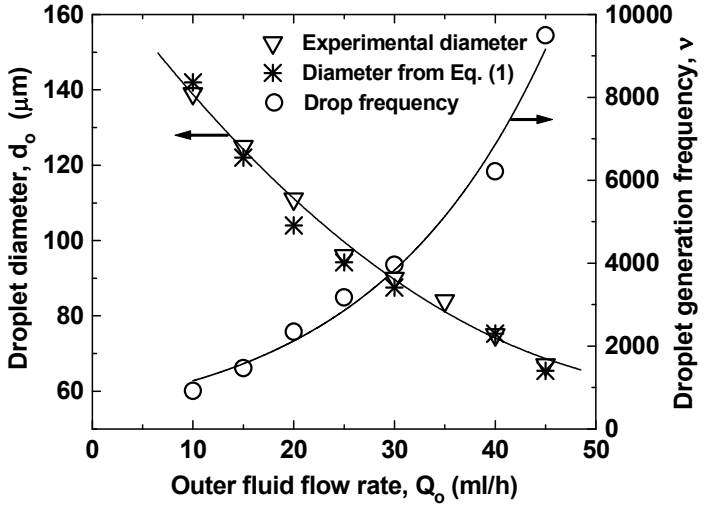


**Figure 3** The effect of outer fluid flow rate on the droplet diameter and generation frequency at $Q_i$ = 4 ml/h and $Q_m$ = 1 ml/h. The solid lines represent the best fit of the experimental data.

**4 Shell thickness of core/shell droplets**

Assuming that the core is at the center of the shell, which is valid for phases with nearly equal densities, the mass balance equation for middle fluid in the dripping regime gives:

$$\delta = [3Q_i/(4\pi \nu)]^{1/3}\{[1+(Q_m/Q_i)]^{1/3} - 1\} \quad (2)$$

where $\delta$ is the shell thickness. Eq. (2) shows that the shell thickness should increase with increasing the flow rate ratio, $Q_m/Q_i$, as shown in Figure 4. At $Q_m/Q_i = 6$, the middle fluid extends into a long jet before forming a shell around a water droplet. At $Q_m/Q_i = 0.25$ and 1.5, the drop diameter was greater than the diameter of the orifice in the collection capillary, resulting in deformation of the droplets in the tapered region and formation of ellipsoidal drops. It is visible in the image at $Q_m/Q_i = 0.25$. If these ellipsoidal drops contain cross-linkable compounds in the shell, they can potentially be transformed into non-spherical particles through polymerisation in the entry region of the collection tube.

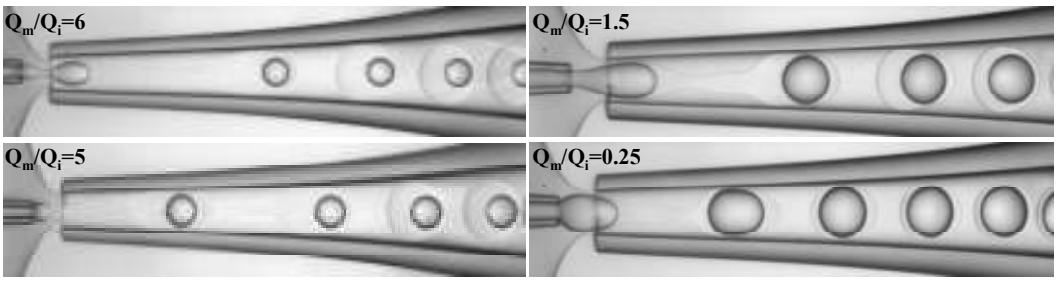


**Figure 4** Still images from high-speed videos showing generation of core/shell droplets with variable shell thickness at different flow rate ratios of the middle to inner phase.

For a given flow rate of the middle and inner fluid, the shell thickness decreases with increasing the outer fluid flow rate, as shown in Figure 5. The minimum shell thickness of 2.4 μm was obtained at the outer fluid flow rate of 45 ml $h^{-1}$ and $Q_m/Q_i = 0.25$. To obtain core/shell droplets with shells in the nanometre region (100 nm or even less), different design of the device should be used with middle fluid delivered through the injection capillary and inner fluid supplied through a small tapered capillary inserted into the injection capillary [19]. In this configuration, the inner and middle fluid form a biphasic flow within the injection capillary and the thickness of the middle fluid can be made very thin because of its high affinity to the wall of the capillary.

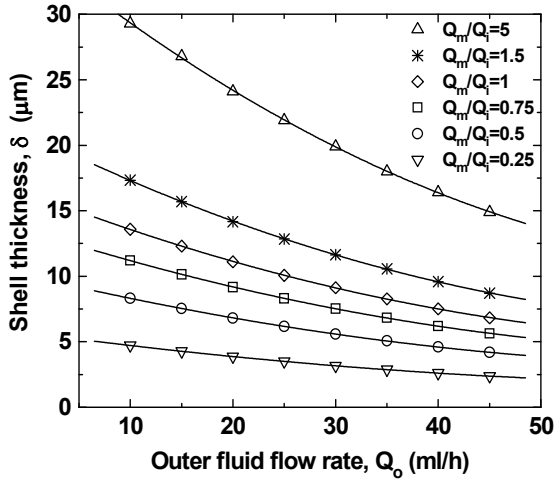


**Figure 5** The shell thickness vs. outer fluid flow rate at different flow rate ratios of the inner to middle fluid, $Q_m/Q_i$. The sum of the middle and inner fluid flow rate was 5 ml $h^{-1}$.

## Conclusions

We have demonstrated the ability of glass microcapillary device that combine co-flow and flow-focusing geometries to generate controllable multiple emulsions. The droplets formed using this device had either core/shell morphology or contained two internal droplets per each outer drop and the dominant regime was controlled by adjusting fluid flow rates. The shell thickness ranged from about 2 μm to several tens of μm and was finely tuned by controlling the flow rate ratio of the middle to inner fluid, $Q_m/Q_i$. The higher the $Q_m/Q_i$ ratio, the thicker the shell around the droplet became. The droplet production rate was controlled by adjusting the flow rate of the continuous phase. The shell material can be polymerised to produce spherical or non-spherical polymer shells or may contain dissolved amphiphilic molecules or particles which can undergo self-assembly upon solvent evaporation, leading to the generation of functional vesicles.

## Acknowledgement

The work was supported by the Engineering and Physical Sciences Research Council (EPSRC) of the United Kingdom (grant reference number: EP/HO29923/1).

## References

1. H. Sawalha, K. Schroën, R. Boom, AIChE J. **55**, 2827 (2009).

2. J.W. Kim, A.S. Utada, A. Fernández-Nieves, Z. Hu, D.A. Weitz, Angew. Chem. Int. Ed. **46**, 1819 (2007).

3. A. Fernández-Nieves, V. Vitelli, A.S. Utada, D.R. Link, M. Márquez, D.R. Nelson, D.A. Weitz, Phys. Rev. Lett. **99**, 157801 (2007).

4. H.C. Shum, D. Lee, I. Yoon, T. Kodger, D.A. Weitz, Langmuir **24**, 7651 (2008).

5. E. Lorenceau, A.S. Utada, D.R. Link, G. Cristobal, M. Joanicot, D.A. Weitz, Langmuir **21**, 9183 (2005).

6. D. Lee, D.A. Weitz, Adv. Mater. **20**, 3498 (2008).

7. P. Walde, S. Ichikawa, Biomol. Eng. **18**, 143 (2001).

8. R.K. Shah, H.C. Shum, A.C. Rowat, D. Lee, J.J. Agresti, A.S. Utada, L.Y. Chu, J.W. Kim, A. Fernandez-Nieves, C.J. Martinez, D.A. Weitz, Mater. Today **11**, 18 (2008).

9. R. Atkin, R. Davies, J. Hardy, B. Vincent, Macromolecules **37**, 7979 (2004).

10. K. Nakagawa, S. Iwamoto, M. Nakajima, A. Shono, K. Satoh, J. Colloid Interface Sci. **278**, 198 (2004).

11. E. Donath, G.B. Sukhorukov, F. Caruso, S.A. Davis, H. Möhwald, Angew. Chem. Int. Ed. **37**, 2201 (1998).

12. J.H. Han, B.M. Koo, J.W. Kim, K.D. Suh, Chem. Commun. **28**, 984 (2008).

13. A.R. Abate, D.A. Weitz, Small **5**, 2030 (2009).
14. A.S. Utada, E. Lorenceau, D.R. Link, P.D. Kaplan, H.A. Stone, D.A. Weitz, Science **38**, 537 (2005).
15. B.J. Sun, H.C. Shum, C. Holtze, D.A. Weitz, ACS Appl. Mater. Interfaces **2**, 3411 (2010).
16. A.S. Utada, A. Fernandez-Nieves, H.A. Stone, D.A. Weitz, Phys. Rev. Lett. **99**, 4 (2007).
17. D. Lee, D.A. Weitz, Small **5**, 1935 (2009).
18. G. Gasparini, S.R. Kosvintsev, M.T. Stillwell, R.G. Holdich, Colloid Surf. B **61**, 199 (2008).
19. S.H. Kim, J.W. Kim, J.C. Cho, D.A. Weitz, Lab Chip **11**, 3162 (2011).

## Figure legends

**Figure 1** (a) Schematic of the glass capillary device used in this work; (b) Micrograph of the tapered end of the injection and collection tube. The diameter of the orifice in the injection and collection tube was 44 and 115 μm, respectively and the distance between the ends of the two capillaries was 90 μm.

**Figure 2** (a) Micrographs of core/shell droplets with $d_o$ = 78 μm and $\delta$ = 8 μm taken under different magnification; (b) Micrograph of multiple emulsion droplets containing two inner drops.

**Figure 3** The effect of outer fluid flow rate on the droplet diameter and generation frequency at $Q_i$ = 4 ml/h and $Q_m$ = 1 ml/h. The solid lines represent the best fit of the experimental data.

**Figure 4** Still images from high-speed videos showing generation of core/shell droplets with variable shell thickness at different flow rate ratios of the middle to inner phase.

**Figure 5** The shell thickness vs. outer fluid flow rate at different flow rate ratios of the inner to middle fluid, $Q_m/Q_i$. The sum of the middle and inner fluid flow rate was 5 ml $h^{-1}$.

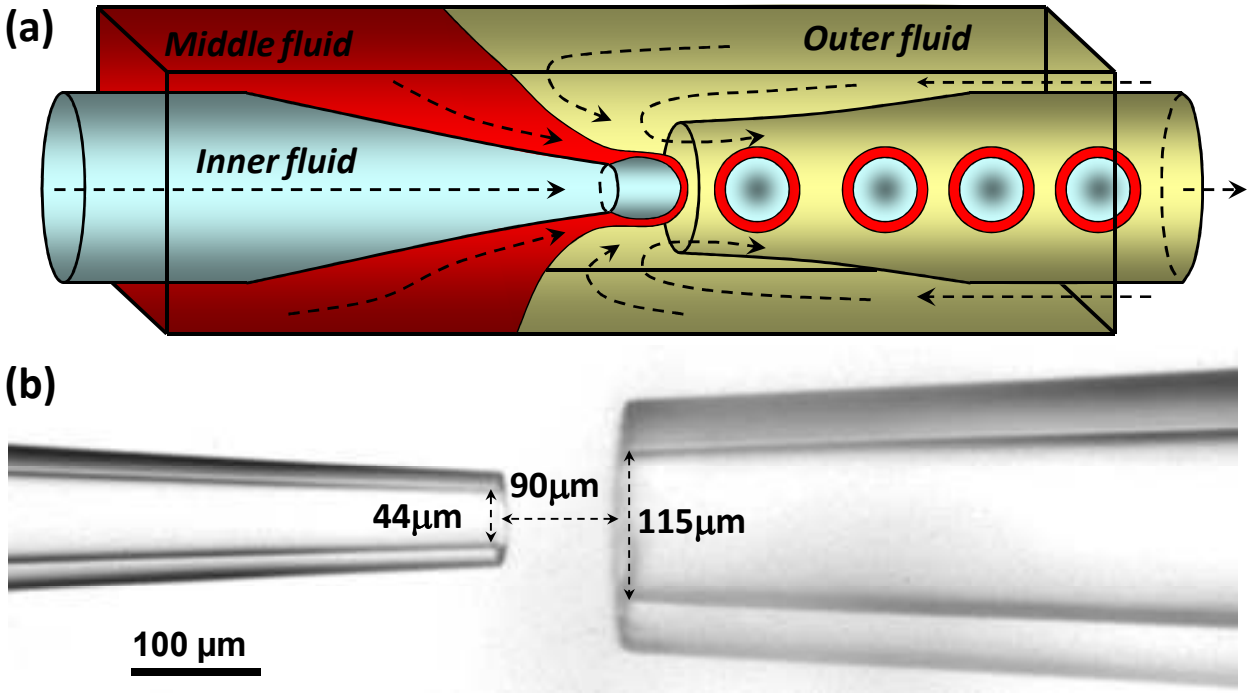


**Figure 1** (a) Schematic of the glass capillary device used in this work; (b) Micrograph of the tapered end of the injection and collection tube. The diameter of the orifice in the injection and collection tube was 44 and 115 µm, respectively and the distance between the ends of the two capillaries was 90 µm.

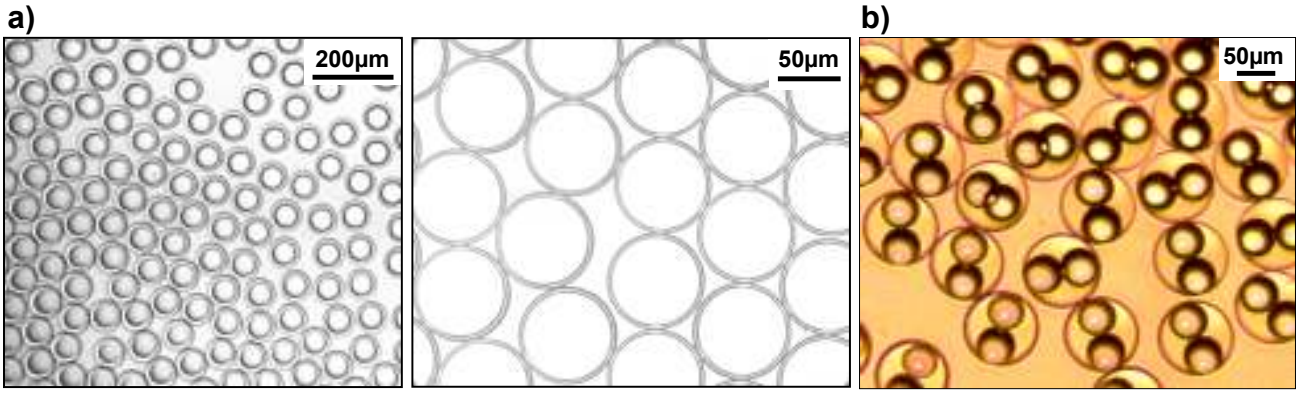


**Figure 2** (a) Micrographs of core/shell droplets with $d_o$ = 78 μm and $\delta$ = 8 μm taken under different magnification; (b) Micrograph of multiple emulsion droplets containing two inner drops.

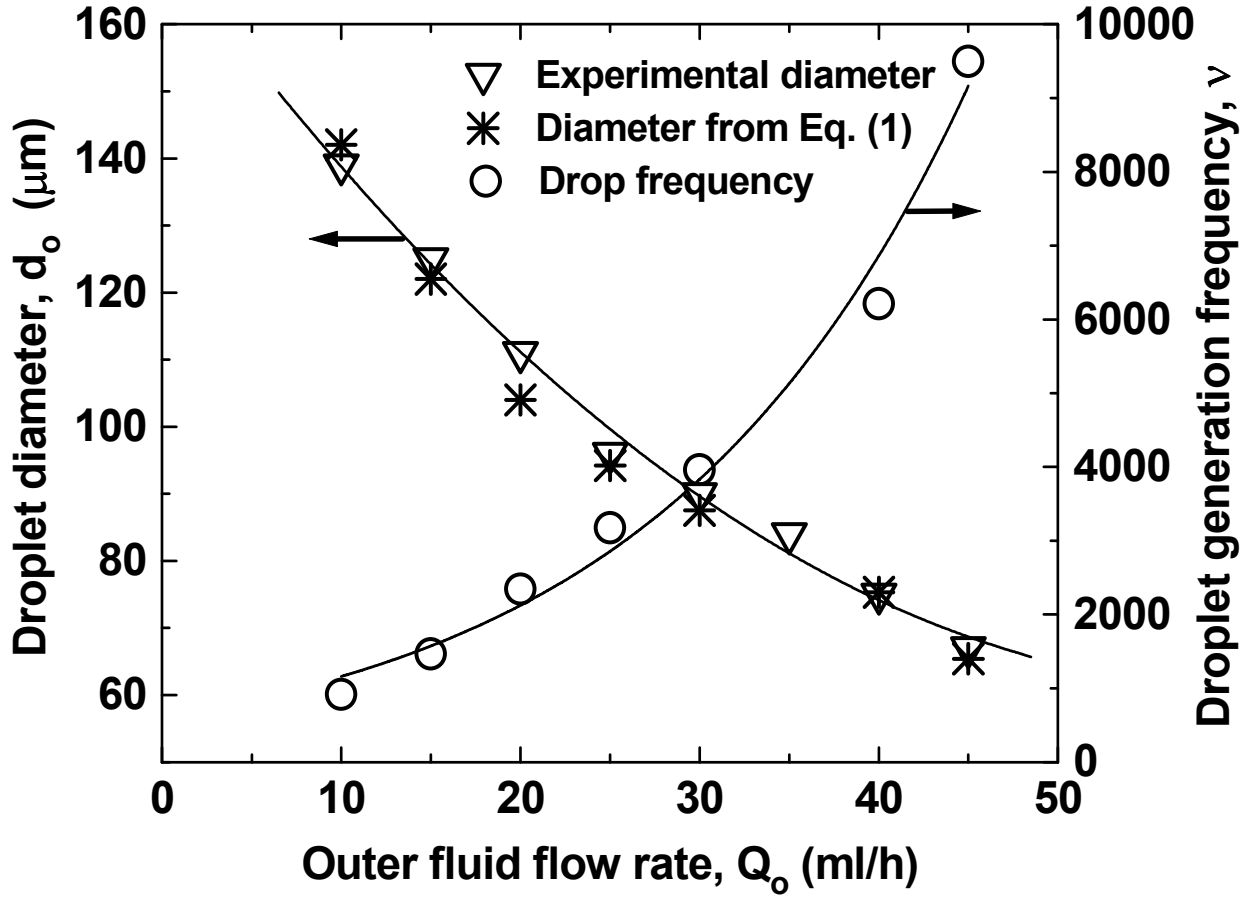


**Figure 3** The effect of outer fluid flow rate on the droplet diameter and generation frequency at $Q_i$ = 4 ml/h and $Q_m$ = 1 ml/h. The solid lines represent the best fit of the experimental data.

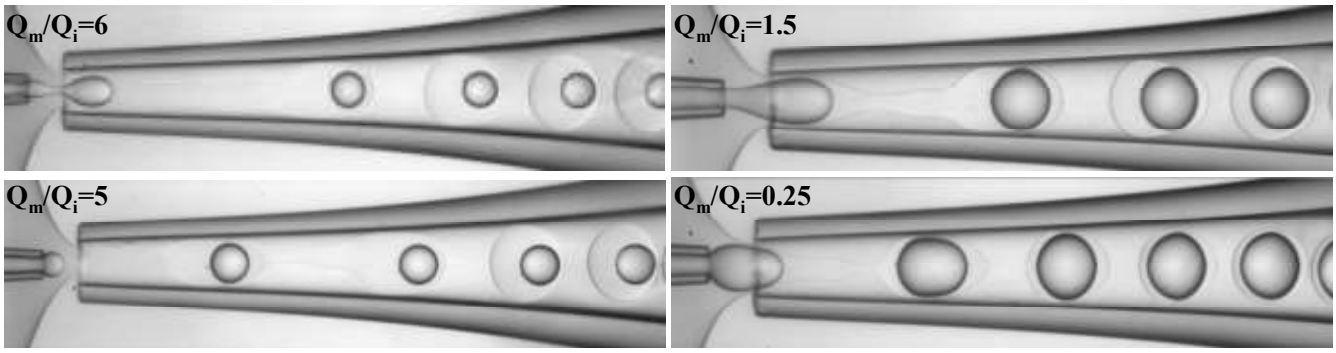


**Figure 4** Still images from high-speed videos showing generation of core/shell droplets with variable shell thickness at different flow rate ratios of the middle to inner phase.

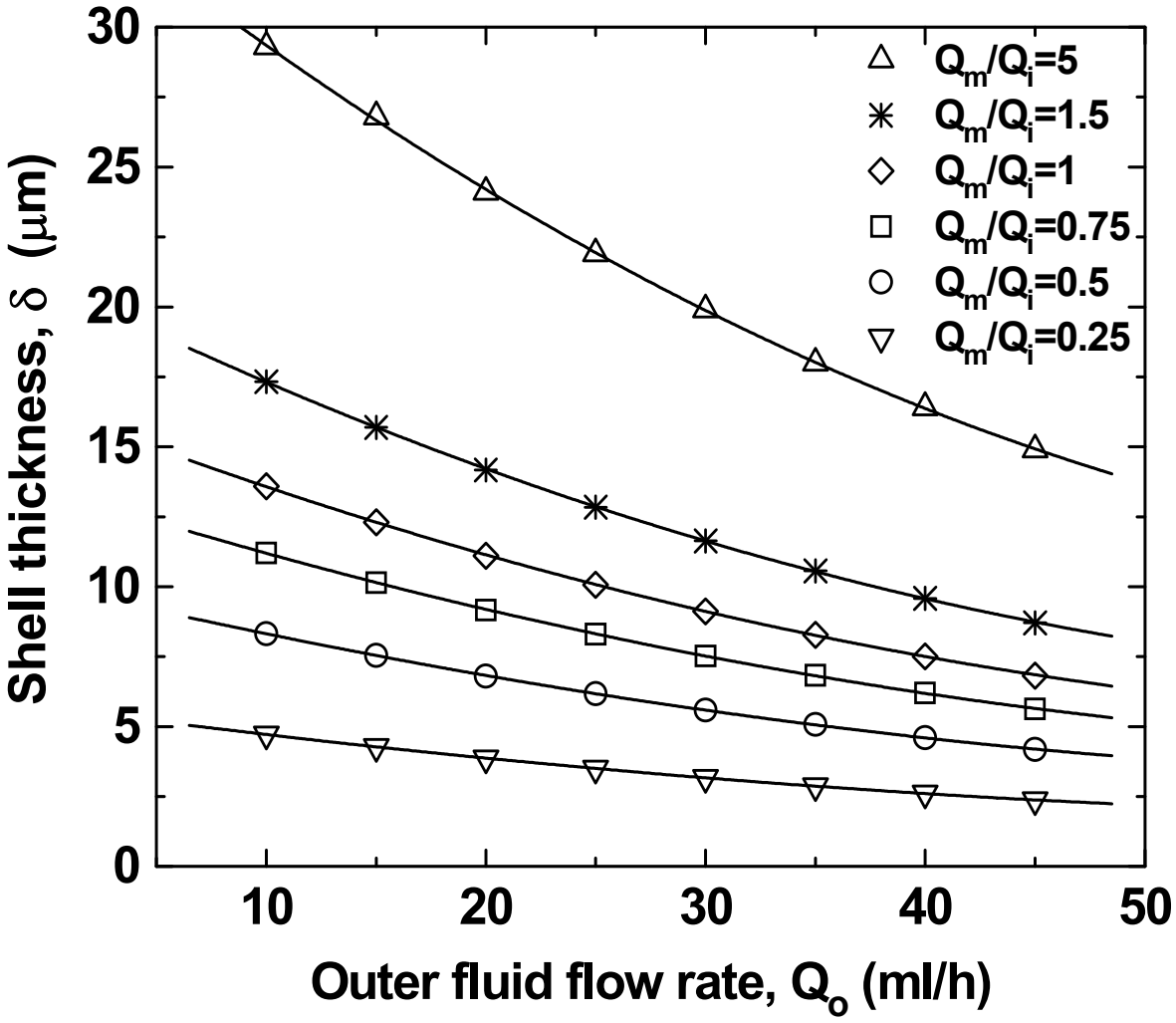


**Figure 5** The shell thickness vs. outer fluid flow rate at different flow rate ratios of the inner to middle fluid, $Q_m/Q_i$. The sum of the middle and inner fluid flow rate was 5 ml $h^{-1}$.